

Predicting optical coherence tomography-derived diabetic macular edema grades from fundus photographs using deep learning

Avinash Varadarajan^{1*}

Pinal Bavishi^{1*}

Paisan Raumviboonsuk, MD^{2*}

Peranut Chotcomwongse, MD^{2†}

Subhashini Venugopalan, PhD^{1†}

Arunachalam Narayanaswamy, PhD^{1†}

Jorge Cuadros, OD, PhD^{3†}

Kuniyoshi Kanai, OD, PhD⁴

George Bresnick, MD³

Mongkol Tadarati, MD²

Sukhum Silpa-archa, MD²

Jirawut Limwattanayingyong, MD²

Variya Nganthavee, MD²

Joe Ledsam, MBChB⁵

Pearse A Keane, MD⁶

Greg S Corrado, PhD¹

Lily Peng, MD, PhD^{1‡**}

Dale R Webster, PhD^{1‡}

¹Google AI, Google, Mountain View, CA, USA

²Department of Ophthalmology, Faculty of Medicine, Rajavithi Hospital, College of Medicine, Rangsit University, Bangkok, Thailand

³EyePACS LLC, Santa Cruz, CA, USA

⁴University of California, Meredith Morgan Eye Center, Berkeley, CA, USA

⁵Google DeepMind, Google, London, UK

⁶NIHR Biomedical Research Centre for Ophthalmology, Moorfields Eye Hospital NHS Foundation Trust and UCL Institute of Ophthalmology, United Kingdom

*Equal Contribution

†Equal Contribution

‡Equal Contribution

**Corresponding Author

Abstract

Diabetic eye disease is one of the fastest growing causes of preventable blindness. With the advent of anti-VEGF (vascular endothelial growth factor) therapies, it has become increasingly important to detect center-involved diabetic macular edema. However, center-involved diabetic macular edema is diagnosed using optical coherence tomography (OCT), which is not generally available at screening sites because of cost and workflow constraints. Instead, screening programs rely on the detection of hard exudates as a proxy for DME on color fundus photographs, often resulting in high false positive or false negative calls. To improve the accuracy of DME screening, we trained a deep learning model to use color fundus photographs to predict DME grades derived from OCT exams. Our “OCT-DME” model had an AUC of 0.89 (95% CI: 0.87-0.91), which corresponds to a sensitivity of 85% at a specificity of 80%. In comparison, three retinal specialists had similar sensitivities (82-85%), but only half the specificity (45-50%, $p < 0.001$ for each comparison with model). The positive predictive value (PPV) of the OCT-DME model was 61% (95% CI: 56-66%), approximately double the 36-38% by the retina specialists. In addition, we used saliency and other techniques to examine how the model is making its prediction. The ability of deep learning algorithms to make clinically relevant predictions that generally require sophisticated 3D-imaging equipment from simple 2D images has broad relevance to many other applications in medical imaging.

Introduction

Diabetic macular edema (DME) is a late stage of diabetic eye disease that is characterized by retinal thickening in the macula, often accompanied by hard exudate deposition, and resultant

vision loss. It is one of the most common reasons for referrals to diabetic eye clinics and affects 3-33% of patients with diabetes.¹ The wide range of prevalences reflects the varied bases for defining the condition as well as the varied composition of the populations studied. Currently, the first-line treatment for macular edema is anti-vascular endothelial growth factor (anti-VEGF) agents.²⁻⁴ To determine eligibility for anti-VEGF treatment of DME, most of the major clinical trials measured macular thickening using optical coherence tomography (OCT), and initiate treatment if a patient met the criteria for a particular type of DME.^{5,6} As such, findings on OCT has become a widely-accepted gold standard for determining DME treatment.⁷

However, despite improvements in therapy, the detection of DME remains a challenge because adding OCTs to the screening process is too costly and logistically difficult to implement widely. Globally, there are 425 million patients with diabetes⁸ and most clinical guidelines recommend that all of them are screened annually.⁹ Currently, selection of patients who may meet treatment criteria is performed during these screenings, which typically utilize monoscopic fundus images. These images are then evaluated for the presence of hard exudates within one optic disc diameter of the center of the macula, a proxy for DME. However, this proxy was developed based on an older standard of care, and some studies have shown that hard exudates have both poor positive predictive value and poor sensitivity for OCT-determined retinal thickening. MacKenzie *et al.* reported that only 42% of patients with hard exudates were found to have DME on OCT,¹⁰ and Wang *et al.* reported that a third of patient-eyes with OCT-detected DME lacked features such as hard exudates on monoscopic fundus photographs.¹¹ Wong *et al* reported a false positive rate of 86.6% for DME screening with existing strategies.¹²

As such, the potential of DR screening for detecting DME is handicapped by an inability to reliably detect DME via human-evaluation of fundus photographs alone.

A potential solution lies in the use of deep learning algorithms, which have been applied to a variety of medical image classification tasks,^{13–15} including for retinal imaging.^{16–19}

Encouragingly, in addition to achieving expert-level performance for grading fundus images, deep learning algorithms are able to make predictions for which the underlying association with fundus images were previously unknown, such as cardiovascular risk factors²⁰ and refractive error.²¹ Thus, we hypothesized that deep learning could be leveraged to directly predict the OCT-derived DME grade using monoscopic fundus photographs.

Results

To train and validate the model, cases were gathered retrospectively from the Rajavithi Hospital in Bangkok, Thailand. Because these cases were gathered from those referred into the retina clinic for further evaluation, the disease distribution is consistent with a population presenting to specialty clinics, and enriched for more severe disease as compared to a DR screening population. Details of the development and clinical validation datasets are presented in Table 1. The development dataset consisted of 6,039 images from 4,035 patients. For some patients only one eye was included because the fellow eye fell under the exclusion criteria. A model was then trained with the OCT-derived label for referable DME as the reference standard (“OCT-DME model”). Referable DME was conservatively defined as center point thickness $\geq 250 \mu\text{m}$ measured via manual caliper measurements excluding the retinal pigment epithelium.^{22,23} A separate model that was trained to predict the presence of hard exudates was also used for

comparison (“HE-DME model”).¹⁸ Both models used fundus photographs as input; but were trained to predict different labels: DME derived from OCT versus DME assessed using hard exudates in fundus images (Figure 1).

The OCT-DME model showed the higher performance in detecting cases with and without DME from monoscopic fundus images when compared to the HE-DME model as well as manual grading (Table 2 and Figure 2). For Referable DME, the OCT-DME model had an AUC of 0.89 (95% CI: 0.87-0.91) and the HE-DME model had an AUC of 0.74 (95% CI: 0.71-0.77). The performance of manual grading by three retinal specialists was similar to that of the HE-DME model, with sensitivities ranging from 82-85% and specificities ranging from 45-50%. The performance similarity between the HE-DME model and manual grading also held true if other common criteria for calling DME for monoscopic images were used (Figure S1), such as changing the definition of DME based on the location of the hard exudates. Additional analyses were also performed at other thickness thresholds for referable DME at $\geq 280 \mu\text{m}$ and $\geq 300 \mu\text{m}$, which showed similar or better results compared to the conservative $\geq 250 \mu\text{m}$ cut off point without model retraining (Figure S2). When compared to manual grading, the OCT-DME model had a 30-35% absolute higher specificity at the same sensitivity ($p < 0.001$ for comparison with each retina specialist). When matched to have the same specificity, the model had a 11-14% absolute higher sensitivity (96% vs. 82-85%, $p < 0.001$ for all comparisons). Results were similar for detecting the presence of intraretinal and subretinal fluid (Figure 3).

In addition to the primary validation dataset, the model was also applied to a secondary validation dataset, EyePACS-DME, to examine the model’s generalizability. This dataset consists of 990 images with moderate or severe non-proliferative DR, or proliferative DR, a

subset of data previously gathered during another DME study.²⁴ The images were gathered using a Canon CR-DGi camera and OCTs were taken with a Optovue iVue machine from a U.S.-based population (see methods). There are some notable differences in this dataset in comparison to the primary validation dataset, particularly in terms of defining and measuring referable DME based on central subfield thickness and incorporation of inclusion/exclusion criteria. Based on this different definition and inclusion criteria, the number of referable cases in this dataset was 7.8% vs 27.2% in the primary validation set. Thus, the model performance on the datasets cannot be compared directly in terms of absolute values. However, relative comparisons between the model and graders (in this instance EyePACS certified graders) can be drawn. Similar to the results of the primary validation, the OCT-DME based model had a positive predictive value (PPV) roughly twice that of manual grading using hard exudates as proxy (35% [95% CI: 27%-44%] vs 18% [95% CI: 13%-23%]) and similar NPV (96% [95% CI: 95%-98%] vs 95% [95% CI: 94%-97%]). This translated to a similar sensitivity (57% [95% CI: 47%-69%] vs 55% [43%-66%]) but higher specificity (91% [95% CI: 89%-93%] vs 79% [95% CI: 76%-82%]). The HE-based model performed on par with manual grading with a sensitivity of 56% (95% CI: 46%-68%) and a specificity of 79% (95% CI: 76%-82%).

Subsampling experiments, where new models were trained using titrated fractions of the dataset, showed that model performance continued to increase without leveling off with larger training sets (Figure 3). These results suggest that the accuracy of this prediction will likely continue to increase with dataset sizes greater than the numbers included in this study. This was true for all prediction tasks -- i.e. referable DME (defined by center point thickness ≥ 250), the presence of intraretinal fluid, and the presence of subretinal fluid.

Results from our model explanation methods are presented in Figure 4 and 5. Based on the heat maps generated by the GradCAM²⁵ method in Figure 4, the HE-DME model (middle column) tends to focus on regions with hard exudates, whereas the model trained on OCT-derived grades (rightmost column) focuses more on the macula.

Figure 5 presents an analysis of which portions of the image are relevant for the OCT-DME model. When the OCT-DME model is trained on cropped fundus images containing only 0.25 optic disc diameter around the fovea (blue line), it already achieves an AUC of 0.75, and when it has access to 1.0 optic disc diameter around the fovea, the model achieves an AUC greater than 0.85, comparable with its performance on the full fundus image. However, the model trained on the region around the optic disc needs to see a lot more context (2.5 optic disc diameter) around the optic disc center to achieve an AUC exceeding 0.8.

Discussion

While the potential of deep learning to make novel predictions has been reported in literature,^{20,21} this study is among the first robust examples of a model far exceeding expert performance for a task with high clinical relevance and potentially important implications for screening programs worldwide. Preliminary secondary validation results also suggest that these results may generalize to other datasets. DME is the major cause of visual loss from DR. Prior to the use of anti-VEGF injections, the Early Treatment of Diabetic Retinopathy Study (ETDRS) showed that treatment of a subtype of DME with focal laser photocoagulation decreased the chance of vision loss.²⁶ Today, with anti-VEGF injections, the treatment of centrally involved

DME can *improve* vision by approximately 10-13 letters as measured using the ETDRS visual acuity chart.⁵ Anti-VEGF injections are now largely considered the gold standard of care with evidence that shows that delaying treatment of DME could lead to suboptimal visual improvement. However, the current grading guidelines in screening programs were developed before the advent of anti-VEGF therapy and are not specifically designed for detecting center-involved diabetic macular edema. The development of models that can better detect DME in DR screening programs using existing equipment (color fundus cameras) is both scientifically interesting and clinically impactful.

For DR screening in particular, this new model of DME screening may lead to fewer false negatives for DME. Decreasing missed referrals for patients with centrally involved DME but with no hard exudates is a clear advantage of such a system. In addition, decreasing false positives is also important in resource-constrained settings. While many screening programs recommend closer follow up for patients with mild or worse DR (i.e. patients with only microaneurysms and hard exudates), the urgency of follow up varies widely, ranging from up to 12 months for moderate nonproliferative DR with no macular edema, to 3-6 months if there is macular edema and 1 month when there is clinically significant macular edema (American Academy of Ophthalmology Recommendation).²⁷ The referral of patients with moderate non-proliferative DR without DME (but with hard exudates) can be an issue where there are limited resources for evaluation and treatment. In addition, the OCT-DME model seems to be also able to detect the presence of intraretinal and/or subretinal fluid, both of which merit closer monitoring and possibly treatment. The ability to detect these pathologies is also somewhat unexpected as this is not a task that doctors can do accurately from fundus images.²⁸ While the

models trained in this study are more accurate than manual grading, there is still room and capacity for improvement. Given the results of the subsampling experiments, it is likely that the accuracy of the model may continue to increase with larger dataset sizes.

From a scientific point of view, this work not only demonstrates the potential of deep learning to enable diagnostics from inexpensive hardware that was only previously possible from expensive equipment but also lays the groundwork for understanding how the model makes these predictions. For example, the explanation techniques employed in this study both indicated that the region around the fovea is more relevant than the region near the optic disc for DME prediction from fundus images. Future studies could leverage these strategy of using multiple explanation techniques to elucidate the most important parts of the image and provide transparency on model decision making.

Despite these promising results, there are a few limitations to this study. First, this study does not evaluate cases without central involvement that meet an older criteria for treatment known as clinically significant macular edema. In a small non-randomized study, Scott *et al.*²⁹ showed a beneficial effect of focal and grid laser for these eyes, similar to the initial ETDRS findings. These patients should still be referred from a DR screening program for closer follow up. To address this, one would include stereoscopic imaging in addition to OCT as ground truth to train model(s) to specifically identify these cases. In addition to training with a larger dataset, the models can be validated with additional larger datasets from other settings, including screening settings from other regions or geographies. While there is some preliminary evidence of generalization to secondary datasets, the confidence intervals are wide and the criteria for referable DME for the EyePACS-DME dataset were different from those of the Thailand dataset.

Future studies should include better standardization for referable DME and inclusion/exclusion criteria as well as sub-analysis of patients who were treated for DME. Some of the performance metrics reported in this study such as positive predictive value (PPV) and negative predictive value (NPV) are relevant only to populations whose severity distribution is similar to that of this study (e.g. patients referred to specialist clinics). Additional work would need to be done to evaluate model performance on screening populations. Moreover, additional data diversity such as the use of DME labels derived from other OCT devices by other manufacturers should be included in future work. The model was trained using a single fundus image. Thus, additional work should be done to see how the model performs on multiple images per eye (including with stereo pairs), and on previously treated eyes. Lastly, future work could also include health economic analysis to demonstrate study the cost-effectiveness of such an approach.

Nevertheless, this study demonstrates that deep learning can be leveraged to identify the presence of OCT-derived DME using the cheaper and more-widely available fundus photograph, at an accuracy exceeding that of manual grading using expert-derived rules. Similar approaches could be particularly valuable for other medical images, such as using radiographs or low-dose computed tomography to detect conditions that would otherwise require more expensive imaging techniques that expose patients to higher radiation doses. Importantly, we show that model explanation techniques can be leveraged to explain how the model is making these new predictions, lending confidence that the predictions will generalize to new unseen datasets.

Methods

This study was approved by the Ethics Committees or Institutional Review Boards of hospitals or health centers where retinal images of patients with diabetes were used in this study, including the Rajavithi Hospital (Bangkok, Thailand), Alameda Health Service (Alameda, CA, USA), and the University of California, Berkeley (Berkeley, CA, USA). Patients gave informed consent allowing their retinal images to be used. This study was registered in the Thai Clinical Trials Registry, Registration Number TCTR20180818002.

Datasets

For algorithm development, 7,072 images were gathered retrospectively from diabetic patients presenting to the retina clinic at Rajavithi Hospital in Bangkok, Thailand from January 2010-February 2018. Only cases that were naive to treatment (both intravitreal injections and lasers) were included. Cases where macular lesions may interfere with the diagnosis of DME, such as idiopathic epimacular membrane, macular edema from other causes, or proliferative DR with neovascular membrane affecting the macula, were excluded from analysis.

Retinal fundus images were obtained using Kowa color fundus camera (VX-10 model, Kowa, Aichi, Japan). A single macula-centered color fundus photograph per eye was used in the study. If available, imaging from both eyes were included. OCTs were obtained using the Heidelberg Spectralis OCT (Heidelberg Engineering GmbH, Germany) and thickness measurements were measured manually (see below for measurement procedures).

Of the 7,072 images in the dataset, 6,039 were used for development while 1,033 were set aside for clinical validation. All images from a patient was present in either in development or validation sets, but not both. Fundus photographs in the validation set were manually graded

by U.S. board-certified retinal specialists to assess the presence and location of hard exudates (yes, no, ungradable, within 500 μm or 1 disc diameter or 2 disc diameter from the center of the macula) and focal laser scars. In addition, retina specialists provided their best clinical judgement of the presence of DME that took into account all the pathology present in the image.

To study generalizability of the model, the algorithm was applied to another dataset, EyePACS-DME, which is a subset of data that had been previously gathered for another DME study.²⁴ This dataset consisted of 990 macula-centered images from 554 patients with at least moderate DR based on grading by certified EyePACS graders (to roughly match the population of those who would be presenting to a retina clinic). No other exclusion criteria were applied to this dataset (e.g. exclusion of epiretinal membrane, etc). Fundus images were taken with a Canon CR-DGi camera (Ōta, Tokyo, Japan) and OCTs were taken with a Optovue iVue machine (Fremont, CA, USA).

Measurement and assessment of OCT scans

To define the reference standard for the presence or absence of DME, OCT was used. For the dataset from Thailand, central subfield thickness, the value representing the thickness of the center of the macula in clinical trials for DME,²³ was not available in all eyes in the developmental dataset, center point thickness, which was found to have high correlation with the central subfield thickness and should be considered as equivalent,²² was therefore measured for each eye to represent the thickness of the center of the macula.

The center point thickness of an eye of a patient was manually measured on the axis of the OCT scan where there were slight elevation of the ellipsoid zone and the widest gap between

the photoreceptor layer outer segment tip and the ellipsoid zone, indicating the center of the fovea where the cone cell density is the highest. Manual measurement was conducted using the straight-line measurement vector available with the Spectralis Eye Explorer software. The vector was put perpendicular to the highly reflective band of retinal pigment epithelium with one side of the vector rested on the highly reflective line of cone outer segment tip and the other side on the internal limiting membrane. Retinal pigment epithelium thickness was not included in this measurement. Intraretinal fluid was defined as present when an obvious cystoid space of hypo-reflectivity was found within 500 μm of the foveal center of any OCT scans of a patient. Subretinal fluid was defined as present when an obvious space of hypo-reflectivity was found between the retina and retinal pigment epithelium within 500 μm of the foveal center of any OCT scans of a patient.

The measurement of center point thickness and the assessment of presence of intraretinal fluid and subretinal fluid were conducted by 2 medical doctors experienced in clinical research and supervised by retinal specialists. 5% of patients were randomly selected to confirm all three measurements by a retinal specialist with 20 years of post-certification experience.

Eyes were divided into cases of no DME and referable for DME. Referable for DME was conservatively defined as eyes with $\geq 250 \mu\text{m}$ center point thickness, excluding the retinal pigment epithelium based upon manual measurement.^{22,23} In addition to the center point thickness-based criteria, we also trained the model in a multi-task fashion to predict subretinal fluid and intraretinal fluid (details below). While cases with subretinal fluid and intraretinal fluid were not strictly included in the criteria in the clinical anti-VEGF trials for DME, referral for follow-up is warranted for these cases.

For the EyePACS-DME dataset, the manufacturer's automated segmentation algorithm was used to measure central subfield thickness. A cut off of 300 μm central subfield thickness was used as the cut-off point for referable DME based on machine-specific adjustments.³⁰ The presence of intraretinal and subretinal fluid was not included as a criteria for referable DME for this dataset.

Model

Our deep learning algorithm for predicting DME was built using the methods described by Gulshan *et al.*,¹⁶ using the Inception-v3³¹ neural network architecture. Briefly, we used a convolutional neural network³² to predict referable DME (center point thickness $\geq 250 \mu\text{m}$), subretinal fluid presence and intraretinal fluid presence. The input to the neural network was a color fundus photograph, and the output was a real-valued number between 0 and 1 for each prediction, indicating its confidence.

The parameters of the neural network were determined by training it on the fundus images and grades in the development dataset. Repeatedly, the model was given a fundus image with a known referable DME grade as determined by a retina specialist looking at the patient's corresponding OCT ("OCT-DME model"). The model predicted its confidence in whether the fundus image was referable for DME, slowly adjusting its parameters over the course of the training process to become more accurate. Note that the OCT-DME model never sees the actual OCT image during training or validation.

We also trained a second model on a dataset that consists of monoscopic fundus images obtained from patients who presented for DR screening at EyePACS-affiliated clinics, as

described in Krause *et al.*¹⁸ The DME grading was done by graders credentialed by EyePACS.³³ Presence of hard exudates within 1 disc diameter of the center of the macula or the presence of focal laser scars was used as the criteria for referable DME. We refer to this trained model as the “HE-DME model”.

Evaluating the algorithm

To evaluate the performance of the OCT-DME and HE-DME models, we used the receiver operating characteristic curve and calculated the area under the curve (AUC). The performance of the retinal specialists was marked by points on this curve indicating their sensitivity and specificity. The same models were both evaluated at increasing thresholds of thickness for referable DME.

Statistical Analysis

To assess the statistical significance of these results, we used the non-parametric bootstrap procedure: from the validation set of N patients, sample N patients with replacement and evaluate the model on this sample. By repeating this sampling and evaluation 2,000 times, we obtain a distribution of the performance metric (e.g. AUC), and report the 2.5 and 97.5 percentiles as 95% confidence intervals. For statistical comparisons, the permutation test was used with 2,000 random permutations.³⁴

Model Explanation

We also used visual explanation tools to understand which regions in the fundus image our deep learning model used in order to make its decisions. We used GradCAM²⁵, a technique that provides a heat map highlighting regions of the image which strongly influenced the model's prediction (of either DME or no DME). GradCAM does this by measuring, for the parts of the network that can be traced back to a specific location on the image, the relative contributions of that part of the network to the overall prediction. These values can then be overlaid into the image in the form of colored heatmaps to give a visual indicator of the importance of any given region on the image.

We performed two additional experiments to determine which regions in a fundus image are most informative of DME. We focussed on two regions, the macula and the optic disc. We trained and evaluated our model looking only at the region that is within a factor of optic disc diameters around the fovea (or equivalently the optic disc) with the rest of the fundus blacked out. We trained and evaluated different models for different radii, increasing the area that the model looks at to understand the importance of these regions in making the prediction.

Acknowledgements

Dr. Nitee Ratprasatporn, Dr. Withawat Sapthanakorn, Dr. Vorarit Jinaratana, Dr. Yun Liu, Dr. Naama Hammel, Ashish Bora, Anita Misra, Dr. Ali Zaidi, Dr. Courtney Crawford, Dr. Jesse Smith for their assistance in reviewing the manuscript, image grading, and data collection.

Competing interests

The authors are employees of Google.

Figures & Tables

Characteristics	Development Set	Primary Clinical Validation Set
Number of Patients	4035	697
Number of Images	6039	1033
Age: Mean, years (SD)	55.6 (10.8) <i>n</i> =6038	55.8 (10.8) <i>n</i> =1033
Gender (% male)	60.8% <i>n</i> =6036	62.4% <i>n</i> =1031
Center Point Thickness: Mean, μm (SD)	263.8 (146.5) <i>n</i> =6039	258.4 (132.8) <i>n</i> =1033
Referable DME, Center Point Thickness \geq 250 μm	28.3% <i>n</i> =6039	27.2% <i>n</i> =1033
Subretinal Fluid Presence	15.7% <i>n</i> =6039	15.1% <i>n</i> =1033
Intraretinal Fluid Presence	45.5% <i>n</i> =6039	46.3% <i>n</i> =1033

Table 1: Baseline characteristics of the development and primary clinical validation datasets.

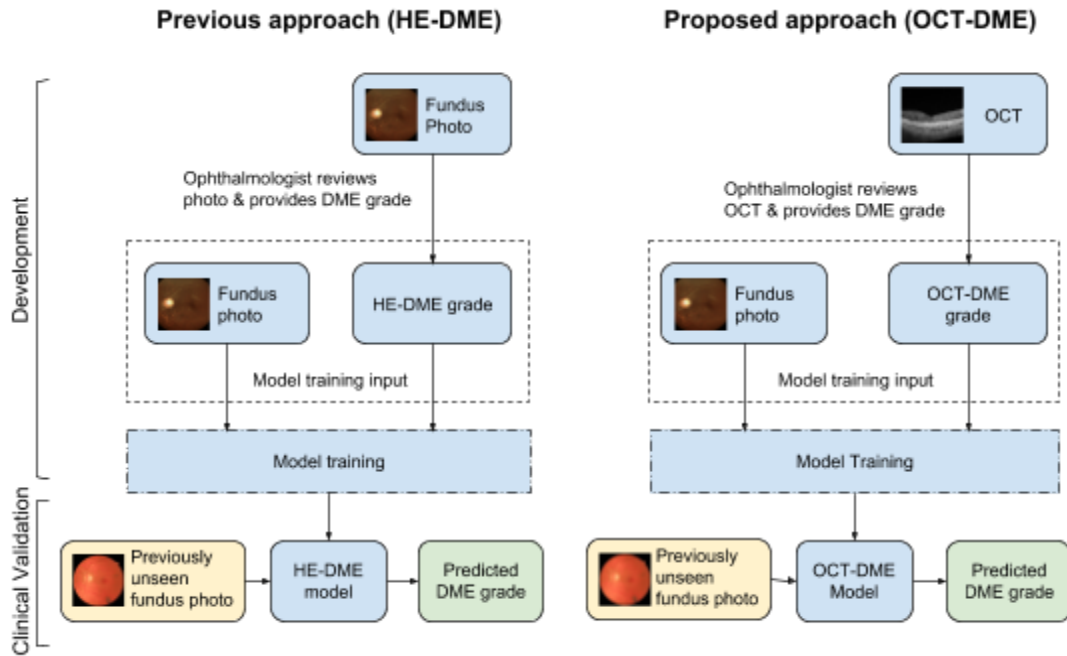


Figure 1. Comparison of our proposed OCT-DME model with the previous approach. Ground truth grades are derived from the analysis of OCT data for each case. These labels (“OCT-DME Grade”) and corresponding color fundus photos are used for model training. For clinical validation, the trained model takes in a new fundus photo and generates a predicted DME grade.

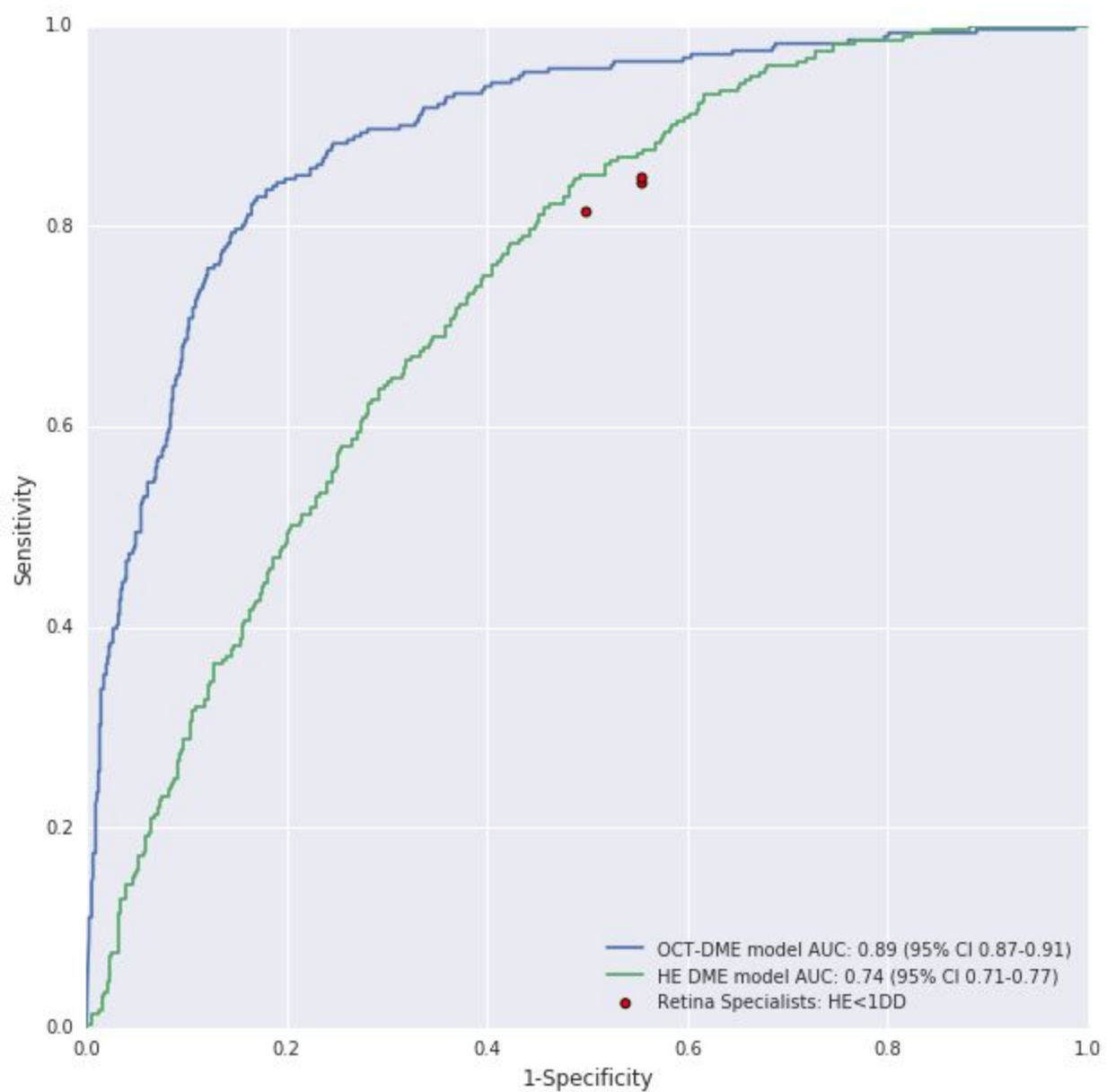


Figure 2: Receiver operating characteristic curve of OCT-DME model and HE-DME model with retina specialists' grades shown as red dots for predicting referable DME. All methods (i.e. the two models and retinal specialists) rendered their grades using monoscopic fundus images only. The ground truth was derived using OCT (center point thickness $\geq 250 \mu\text{m}$).

Metric	OCT model	HE Model	Specialist 1	Specialist 2	Specialist 3
Positive Predictive Value (%), 95% CI	61% [56%-66%] <i>n</i> =1033	39% [36%-43%] <i>n</i> =1033	37% [33%-40%] <i>n</i> =1004	36% [33%-40%] <i>n</i> =987	38% [34%-42%] <i>n</i> =1001
Negative Predictive Value (%), 95% CI	93% [91%-95%] <i>n</i> =1033	90% [87%-93%] <i>n</i> =1033	88% [85%-91%] <i>n</i> =1004	89% [85%-92%] <i>n</i> =987	88% [84%-91%] <i>n</i> =1001
Sensitivity (%), 95% CI	85% [80%-89%] <i>n</i> =1033	84% [79%-88%] <i>n</i> =1033	84% [80%-89%] <i>n</i> =1004	85% [80%-89%] <i>n</i> =987	82% [77%-86%] <i>n</i> =1001
Specificity (%), 95% CI	80% [77%-82%] <i>n</i> =1033	52% [48%-55%] <i>n</i> =1033	45% [41%-48%] <i>n</i> =1004	45% [41%-48%] <i>n</i> =987	50% [47%-54%] <i>n</i> =1001

Table 2: Performance metrics (PPV, NPV, Sensitivity and Specificity) of the new model for predicting OCT-derived DME compared with the HE based model and 3 retina specialists. For both models, we chose an operating point that matched the sensitivity of the retina specialists to calculate Sensitivity, Specificity, PPV and NPV. The performance metrics for the two models were calculated on the entire clinical validation set; for the retina specialists it was calculated only on the images that they marked as gradable. Brackets denote 95% confidence intervals.

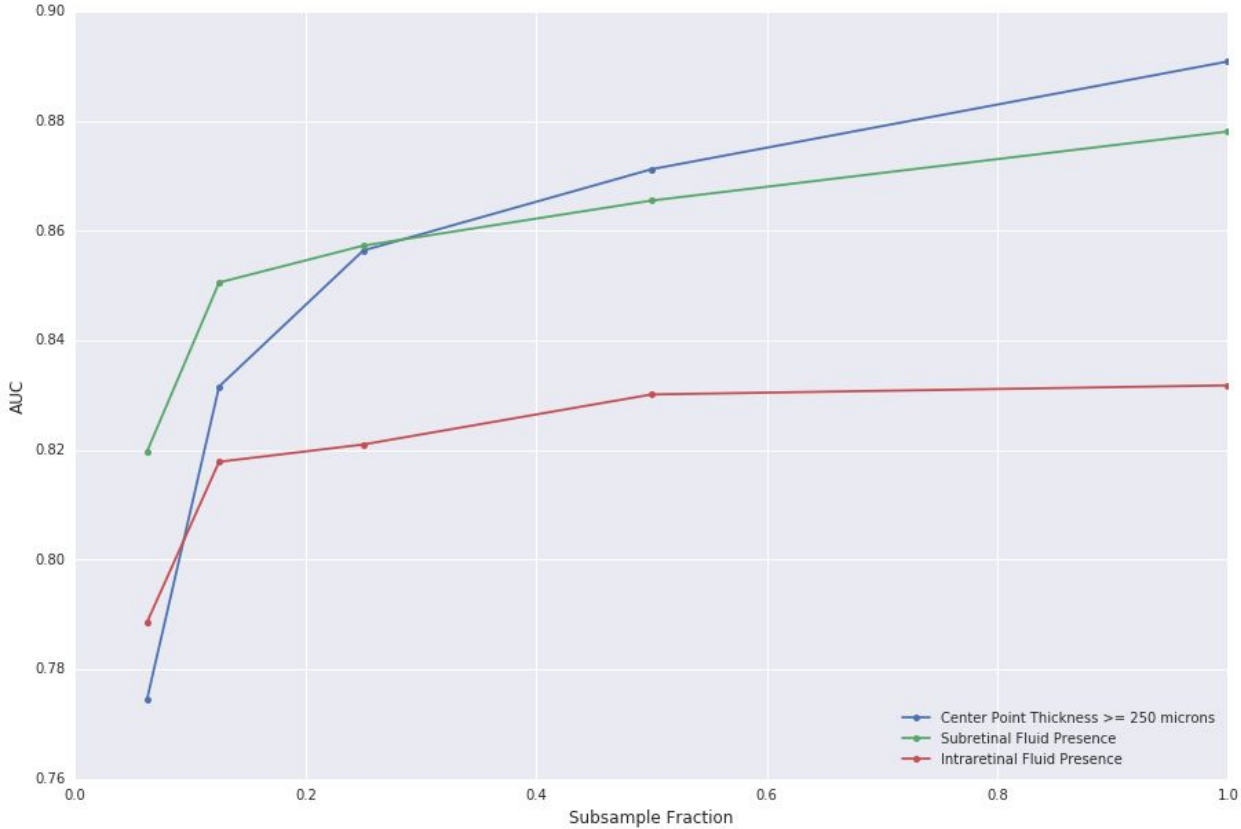


Figure 3. Effect of data size on predicting the different factors that would result in closer follow up for DME including increased center point thickness, presence of subretinal fluid and presence of intraretinal fluid. A subsampled fraction of 1.0 indicates the entire training dataset.

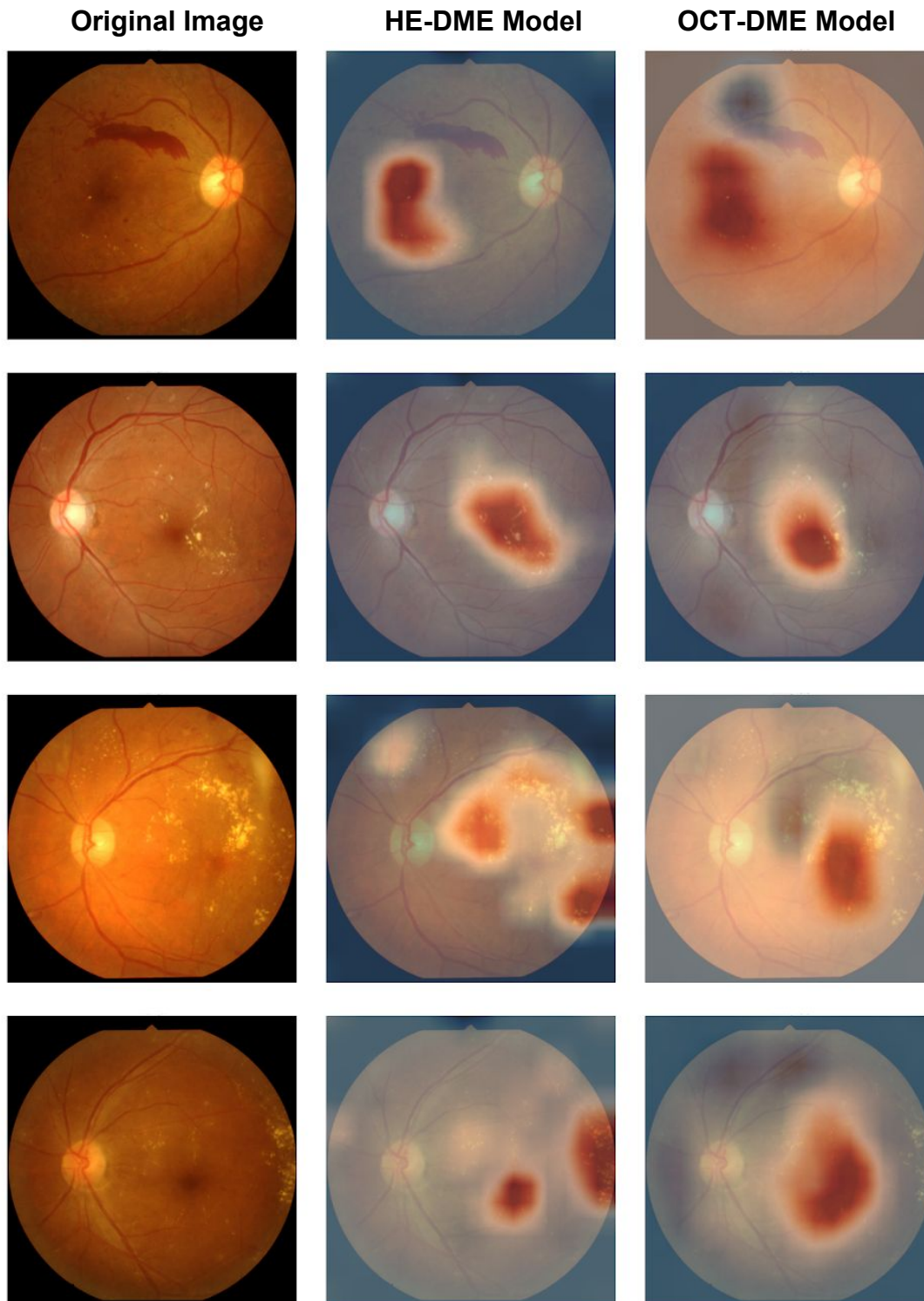


Figure 4. Figure showing five example fundus photos (first column), side-by-side with attention maps generated by applying GradCAM (see Methods) on HE-DME model (second column) and OCT-DME model (third column). All five of these examples had no DME (based on the OCT), despite having prominent hard exudates. Regions highlighted in red on the second and third columns are indicative of the model’s focus when making its predictions. We notice that the focus of the HE-DME model is mostly

on the hard exudates, whereas the OCT-DME model looks primarily at the macula and also sometimes at the hard exudates (last row) while making the decision. In all five of these examples, the HE-DME model made incorrect predictions while the OCT-DME model correctly predicted the absence of DME.

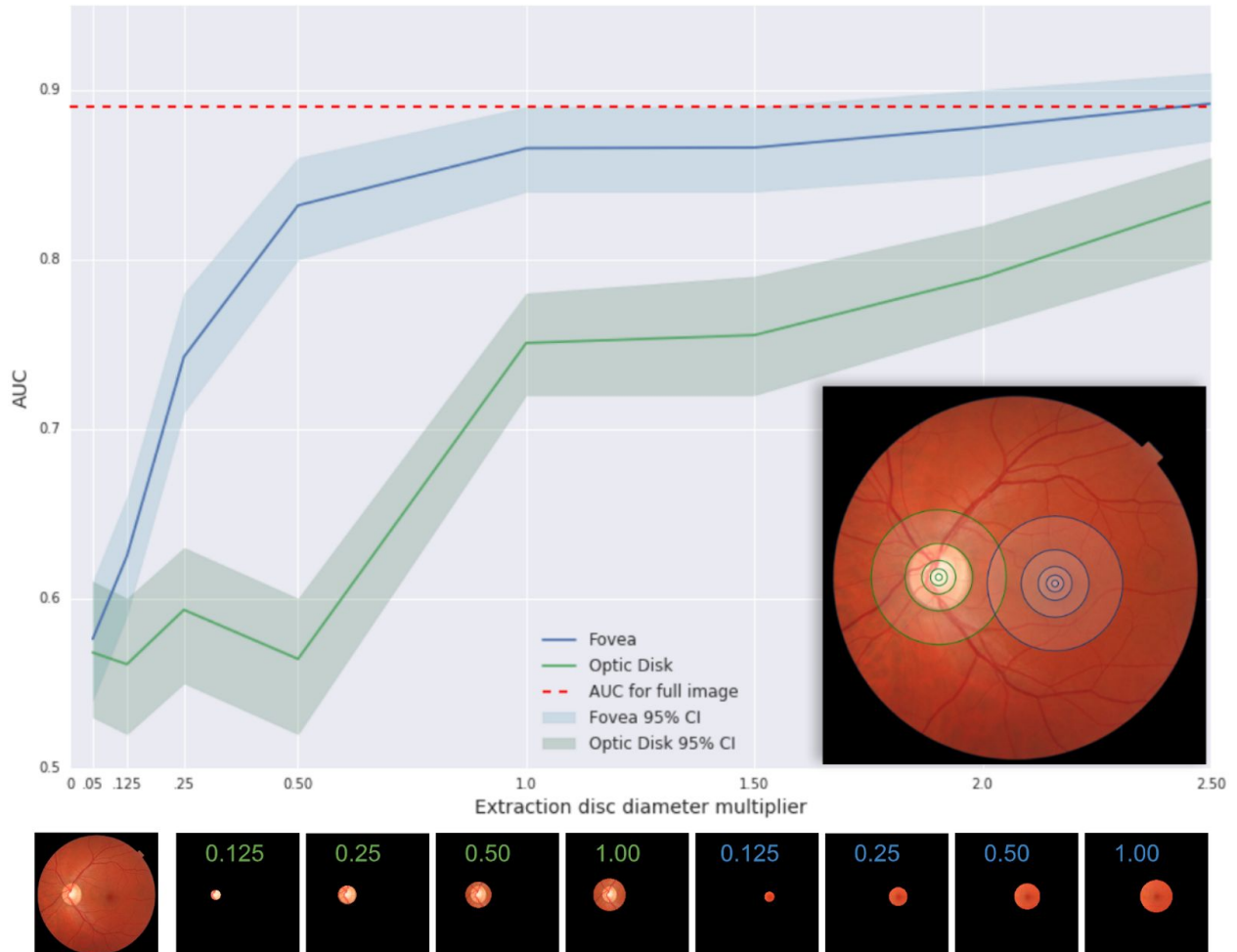


Figure 5: Plot showing model performance as measured by AUC when cropped circular images are used to train and validate the OCT-DME model. The blue line indicates the performance when cropped circular images of different sizes (based on multiples of disc diameter) centered at the fovea are used, while the green line indicates the corresponding performance when the crops are centered at the optic disc. (Inset) Image depicting regions of different radii (0.05, 0.125, 0.25, 0.5, and 1 disc diameter) around the fovea and optic disc. (Bottom panel) Fundus image, followed by the crops extracted by centering at the **optic disc (green)** and **fovea (blue)**, with the extraction disc diameter indicated in each crop.

Supplement

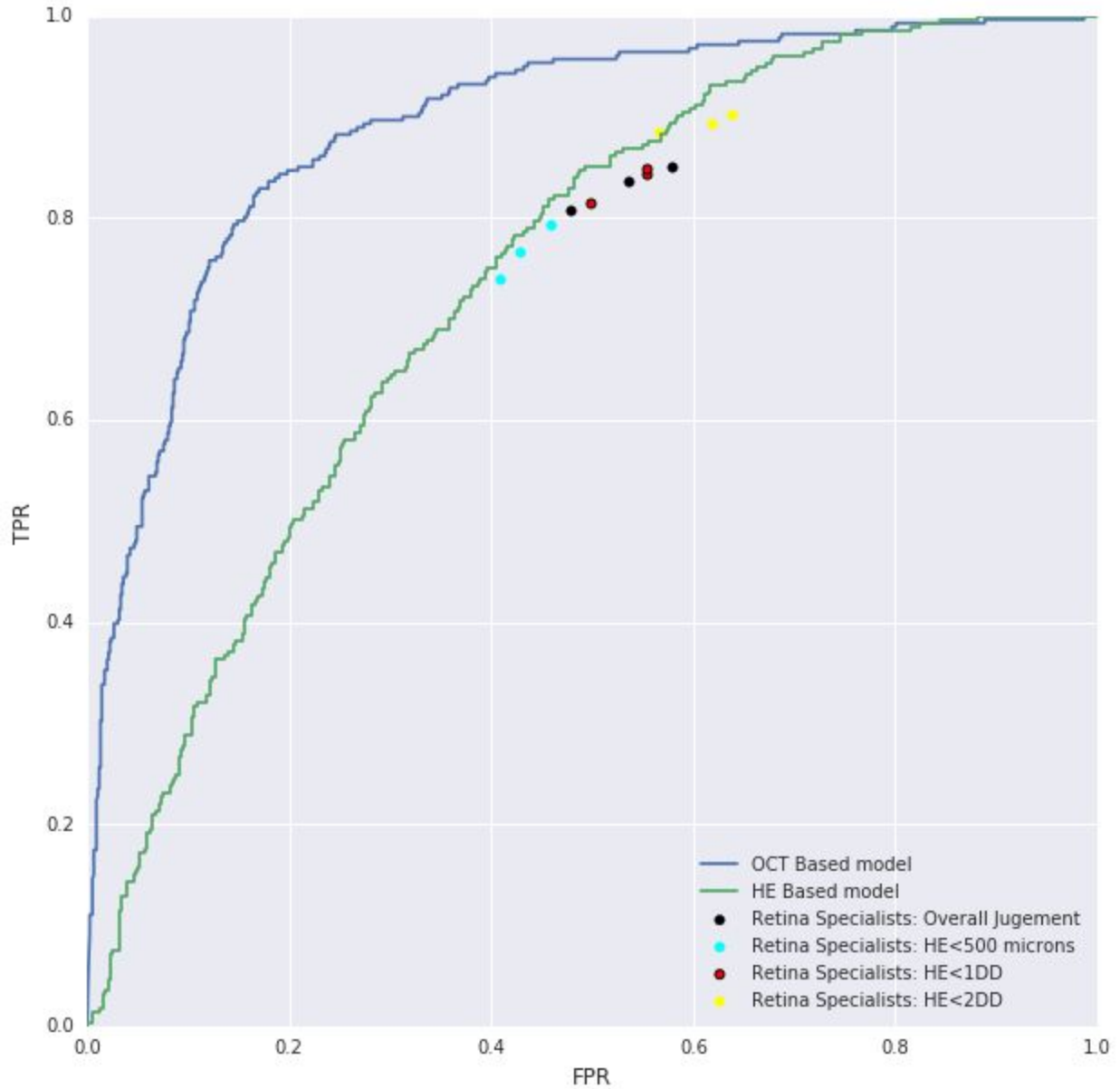
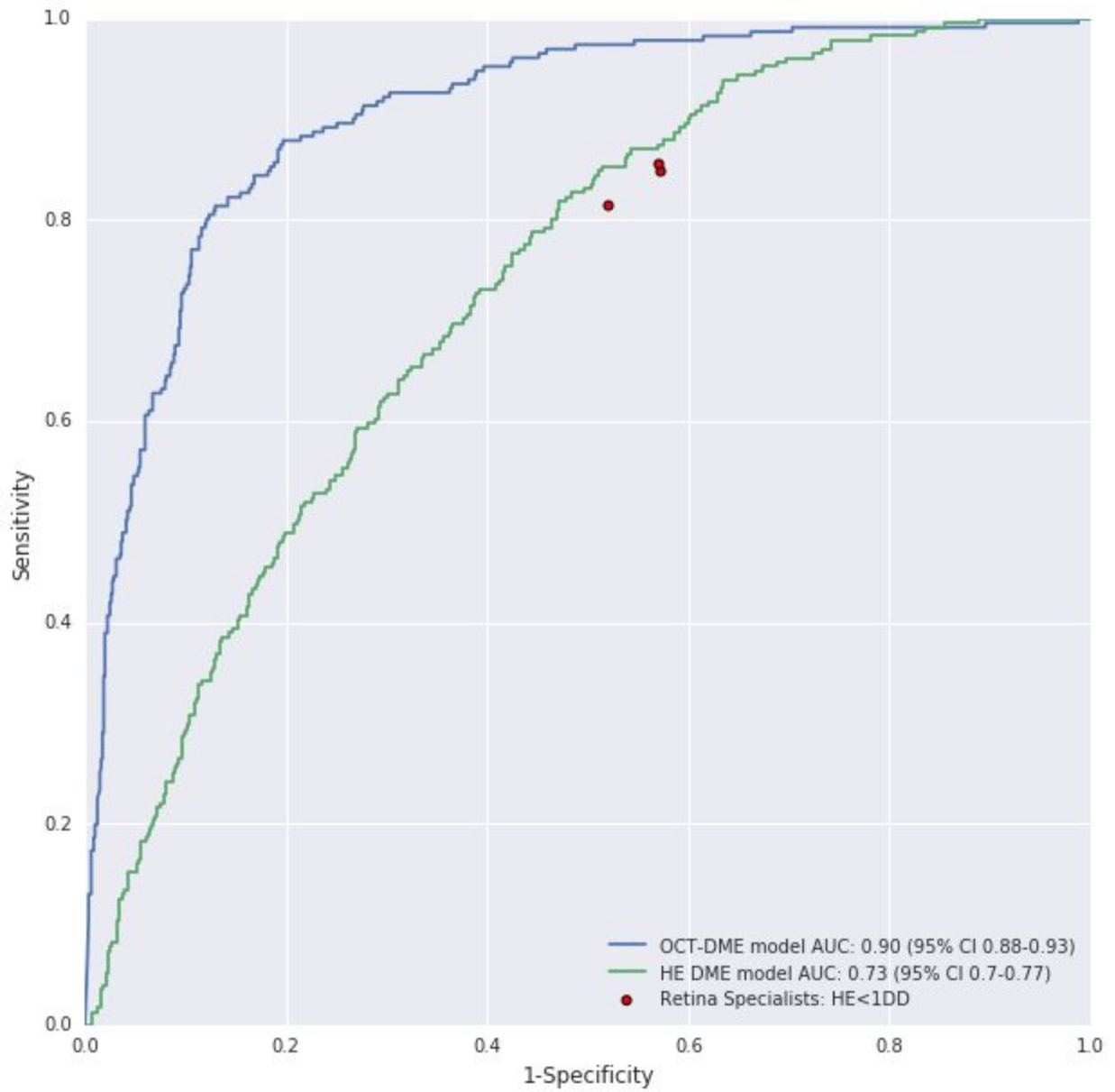
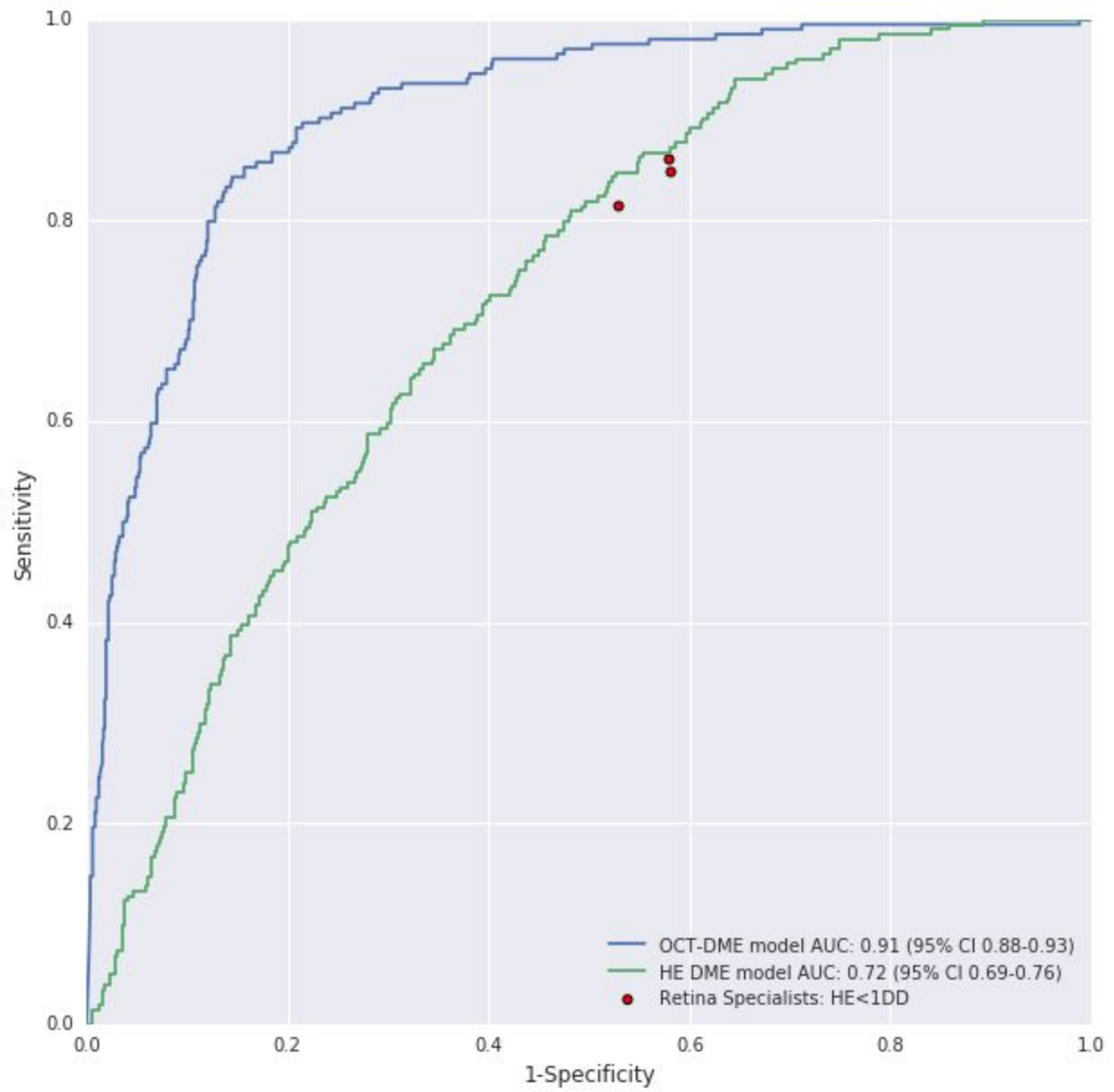


Figure S1: Receiver operating characteristic curve of OCT-DME model and HE-DME model with retina specialists' grades shown as red, yellow, and cyan dots for predicting referable DME using different criteria for manual grading for DME. All methods (i.e. the two models and retinal specialists) rendered their grades using monoscopic fundus images only. The ground truth was derived using OCT (center point thickness $\geq 250 \mu\text{m}$).

A. CPT \geq 280 μ m



B. CPT \geq 300 μ m



C. CPT ≥ 320 μm

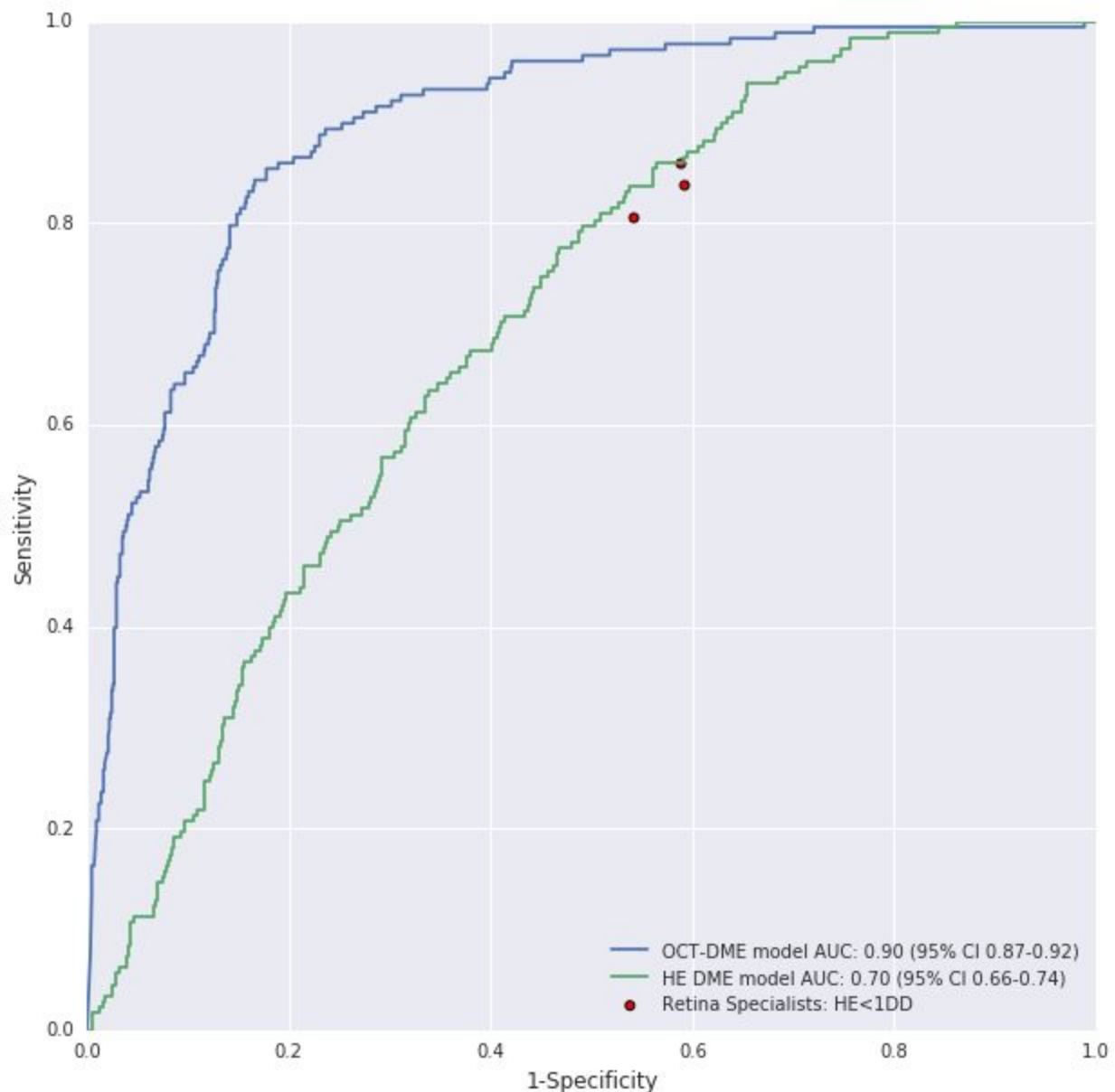


Figure S2: Receiver operating characteristic curve of OCT-DME model and HE-DME model with retina specialists' grades shown as red dots for predicting referable DME. All methods (i.e. the two models and retinal specialists) rendered their grades using monoscopic fundus images only. The ground truth was derived using OCT at different cut off center point thickness for the definition of referable DME. (A) 280 μm , (B) 300 μm , and (C) 320 μm .

Metric	OCT model	HE Model	Specialist 1	Specialist 2	Specialist 3
Positive Predictive Value (%), 95% CI	61% [57%-66%] <i>n</i> =948	39% [35%-43%] <i>n</i> =948	36% [33%-40%] <i>n</i> =948	37% [33%-41%] <i>n</i> =948	38% [34%-42%] <i>n</i> =948
Negative Predictive Value (%), 95% CI	93% [91%-95%] <i>n</i> =948	90% [86%-93%] <i>n</i> =948	88% [85%-92%] <i>n</i> =948	89% [86%-92%] <i>n</i> =948	87% [84%-90%] <i>n</i> =948

Sensitivity (%), 95% CI	85% [81%-89%] <i>n</i> =948	85% [81%-89%] <i>n</i> =948	85% [80%-89%] <i>n</i> =948	86% [82%-90%] <i>n</i> =948	81% [76%-86%] <i>n</i> =948
Specificity (%), 95% CI	80% [77%-83%] <i>n</i> =948	49% [46%-53%] <i>n</i> =948	44% [40%-47%] <i>n</i> =948	44% [40%-48%] <i>n</i> =948	49% [45%-53%] <i>n</i> =948

Table S1: Performance metrics (PPV, NPV, Sensitivity and Specificity) of the new model for predicting OCT-derived DME compared with the HE based model and 3 retina specialists. For both models, we chose an operating point that matched the sensitivity of the retina specialists to calculate Sensitivity, Specificity, PPV and NPV. The performance metrics for the two models were calculated on the entire clinical validation set. For retina specialists, performance metrics were calculated only on the images that all 3 retina specialists deemed gradable. Brackets denote 95% confidence intervals.

1. Lee, R., Wong, T. Y. & Sabanayagam, C. Epidemiology of diabetic retinopathy, diabetic macular edema and related vision loss. *Eye and Vision* **2**, 17 (2015).
2. Schmidt-Erfurth, U. *et al.* Guidelines for the Management of Diabetic Macular Edema by the European Society of Retina Specialists (EURETINA). *OPH* **237**, 185–222 (2017).
3. Ajlan, R. S., Silva, P. S. & Sun, J. K. Vascular Endothelial Growth Factor and Diabetic Retinal Disease. *Semin. Ophthalmol.* **31**, 40–48 (2016).
4. Silpa-archa, S. & Ruamviboonsuk, P. Diabetic Retinopathy: Current Treatment and Thailand Perspective. *J. Med. Assoc. Thai.* **100 Suppl 1**, S136–47 (2017).
5. Nguyen, Q. D. *et al.* Ranibizumab for diabetic macular edema: results from 2 phase III randomized trials: RISE and RIDE. *Ophthalmology* **119**, 789–801 (2012).
6. Brown, D. M. *et al.* Long-term outcomes of ranibizumab therapy for diabetic macular edema: the 36-month results from two phase III trials: RISE and RIDE. *Ophthalmology* **120**, 2013–2022 (2013).
7. Virgili, G. *et al.* The Cochrane Library. (2015). doi:10.1002/14651858.CD008081.pub3
8. User, S. IDF diabetes atlas - Across the globe. Available at:
<http://www.diabetesatlas.org/across-the-globe.html>. (Accessed: 26th September 2018)
9. Chakrabarti, R., Alex Harper, C. & Keeffe, J. E. Diabetic retinopathy management guidelines. *Expert Rev. Ophthalmol.* **7**, 417–439 (2012).
10. Mackenzie, S. *et al.* SDOCT Imaging to Identify Macular Pathology in Patients Diagnosed with Diabetic Maculopathy by a Digital Photographic Retinal Screening Programme. *PLoS One* **6**, e14811 (2011).

11. Wang, Y. T., Tadarati, M., Wolfson, Y., Bressler, S. B. & Bressler, N. M. Comparison of Prevalence of Diabetic Macular Edema Based on Monocular Fundus Photography vs Optical Coherence Tomography. *JAMA Ophthalmol.* **134**, 222 (2016).
12. Wong RL, E. al. Are we making good use of our public resources? The false-positive rate of screening by fundus photography for diabetic macular oedema. - PubMed - NCBI. Available at: <https://www.ncbi.nlm.nih.gov/pubmed/28684650>. (Accessed: 8th October 2018)
13. Esteva, A. *et al.* Dermatologist-level classification of skin cancer with deep neural networks. *Nature* (2017). doi:10.1038/nature21056
14. Liu, Y. *et al.* Detecting Cancer Metastases on Gigapixel Pathology Images. *arXiv [cs.CV]* (2017).
15. Ehteshami Bejnordi, B. *et al.* Diagnostic Assessment of Deep Learning Algorithms for Detection of Lymph Node Metastases in Women With Breast Cancer. *JAMA* **318**, 2199–2210 (2017).
16. Gulshan, V. *et al.* Development and Validation of a Deep Learning Algorithm for Detection of Diabetic Retinopathy in Retinal Fundus Photographs. *JAMA* **316**, 2402–2410 (2016).
17. Ting, D. S. W. *et al.* Development and Validation of a Deep Learning System for Diabetic Retinopathy and Related Eye Diseases Using Retinal Images From Multiethnic Populations With Diabetes. *JAMA* **318**, 2211–2223 (2017).
18. Krause, J. *et al.* Grader variability and the importance of reference standards for evaluating machine learning models for diabetic retinopathy. *Ophthalmology* (2018). doi:10.1016/j.ophtha.2018.01.034

19. Burlina, P. M. *et al.* Automated Grading of Age-Related Macular Degeneration From Color Fundus Images Using Deep Convolutional Neural Networks. *JAMA Ophthalmol.* **135**, 1170–1176 (2017).
20. Poplin, R. *et al.* Prediction of cardiovascular risk factors from retinal fundus photographs via deep learning. *Nature Biomedical Engineering* **2**, 158–164 (2018).
21. Varadarajan, A. V. *et al.* Deep Learning for Predicting Refractive Error From Retinal Fundus Images. *Invest. Ophthalmol. Vis. Sci.* **59**, 2861–2868 (2018).
22. Browning, D. J. *et al.* Optical coherence tomography measurements and analysis methods in optical coherence tomography studies of diabetic macular edema. *Ophthalmology* **115**, 1366–71, 1371.e1 (2008).
23. Wells, J. A. *et al.* Aflibercept, Bevacizumab, or Ranibizumab for Diabetic Macular Edema: Two-year Results from a Comparative Effectiveness Randomized Clinical Trial. *Ophthalmology* **123**, 1351 (2016).
24. Litvin, T. V. *et al.* Improving Accuracy of Grading and Referral of Diabetic Macular Edema Using Location and Extent of Hard Exudates in Retinal Photography. *J. Diabetes Sci. Technol.* **10**, 262 (2016).
25. Selvaraju, R. R. *et al.* Grad-CAM: Visual Explanations from Deep Networks via Gradient-Based Localization. in *2017 IEEE International Conference on Computer Vision (ICCV)* (2017). doi:10.1109/iccv.2017.74
26. Photocoagulation for diabetic macular edema. Early Treatment Diabetic Retinopathy Study report number 1. Early Treatment Diabetic Retinopathy Study research group. *Arch. Ophthalmol.* **103**, 1796–1806 (1985).

27. Diabetic Retinopathy PPP - Updated 2017. *American Academy of Ophthalmology* (2017).
Available at:
<https://www.aao.org/preferred-practice-pattern/diabetic-retinopathy-ppp-updated-2017>.
(Accessed: 25th August 2018)
28. Brown, J. C. *et al.* Detection of Diabetic Foveal Edema: Contact Lens Biomicroscopy Compared With Optical Coherence Tomography. *Arch. Ophthalmol.* **122**, 330–335 (2004).
29. Scott, I. U. *et al.* Effect of focal/grid photocoagulation on visual acuity and retinal thickening in eyes with non-center-involved diabetic macular edema. *Retina* **29**, 613–617 (2009).
30. THE IVUE(TM) NORMATIVE DATABASE STUDY- METHODOLOGY AND DISTRIBUTION OF OCT PARAMETERS. Available at:
<https://www.aaopt.org/detail/knowledge-base-article/ivuetm-normative-database-study-methodology-and-distribution-oct-parameters>. (Accessed: 2nd October 2018)
31. Szegedy, C., Vanhoucke, V., Ioffe, S., Shlens, J. & Wojna, Z. Rethinking the Inception Architecture for Computer Vision. *arXiv preprint arXiv:1502.03167* (2015).
32. Lecun, Y., Bottou, L., Bengio, Y. & Haffner, P. Gradient-based learning applied to document recognition. *Proc. IEEE* **86**, 2278–2324 (1998).
33. Cuadros, J. & Bresnick, G. EyePACS: an adaptable telemedicine system for diabetic retinopathy screening. *J. Diabetes Sci. Technol.* **3**, 509–516 (2009).
34. Chihara, L. M. & Hesterberg, T. C. *Mathematical Statistics with Resampling and R*. (2011).